

# Intermittency via Self-Similarity – An Analytic Example

Mogens V. Melander and Bruce R. Fabijonas

*Department of Mathematics, Southern Methodist University, Dallas, TX 75275*

(Dated: December 21, 2005; revised October 10, 2018)

Turbulence is known to show intermittency. That is, statistical properties vary with the length scale in a way not accounted for by statistical similarity where dimensionless ratios of moments are constant. Intermittency occurs even in the inertial range of isotropic turbulence, where physical intuition calls for a self-similar scale dependence. Perceived as a lack of overall scaling invariance, inertial range intermittency has become known as anomalous scaling. We present an analytic example demonstrating how anomalous scaling and self-similarity in the form of global scaling invariance can coexist within the same statistics. Whether we observe anomalous scaling or self-similarity depends on which variables we consider. Our example illustrates consequences of a symmetry, but is not meant as an intermittency model.

PACS numbers: 47.27.Eq, 47.52.+j, 11.80.Cr, 47.27.Gs, 05.45.Jn, 47.27.Jv, 47.27.eb, 47.27.ed

Intuitively, fundamental insight is lacking if ‘anomalous’ best describes turbulence in its most ideal form. Theoretically, turbulence is ideal when all simplifying circumstances are present. First, the fluid is incompressible and has constant properties—so the motion obeys the incompressible Navier-Stokes equations. Second, there are no boundaries and the turbulence is homogeneous and isotropic—so there is statistical independence of location and orientation. Third, steady large scale forcing puts the turbulence in equilibrium and makes its properties independent of time. Finally, the Reynolds number is high so that a wide range of scales separates forcing at the long lengths from dissipation at the short lengths. Inertial forces alone govern the physics in this “inertial range.” Physical intuition dictates that the scale dependence in the inertial range must be self-similar—in some global way. That is, full knowledge of the statistics at one scale should suffice to generate the statistics at all other scales.

Kolmogorov<sup>1</sup> (K41) proposed a similarity like that in a Brownian motion where dimensionless ratios of moments are constant. Applied to the difference  $\delta v(\ell)$  in a velocity component over a distance  $\ell$ , this so-called statistical similarity requires  $\langle \delta v^p \rangle / \langle \delta v^2 \rangle^{p/2}$  to be independent of  $\ell$  as suggested by dimensional analysis. Statistical similarity, however, does not agree with the evidence.<sup>2</sup> The moment ratios are not constant. Equivalently, the probability density functions (pdf’s) for  $\delta v(\ell)$  at various  $\ell$  do not collapse to one when plotted in units of standard deviations. Instead, one observes intermittency: fluctuations of many standard deviations become increasingly more likely at smaller  $\ell$ . Correspondingly, the tails of the pdfs flare out and become thicker. Although the moments are power laws, e.g.,  $\langle \delta v^p \rangle \propto \ell^{\zeta_p}$ , the exponent  $\zeta_p$  varies non-linearly with the order  $p$ . In contrast, statistical similarity requires that  $\zeta_p$  be linear. The name “anomalous scaling” alludes to historical frustrations in understanding why statistical similarity fails. Frisch<sup>2</sup> presents an account of the history and theories for intermittency. Kolmogorov<sup>3</sup> addressed the issue with his log-normal model (K62). Although K62 has fallen out

favor, it remains among the best-known intermittency models. To a large extent, it accounts for the discrepancies between the K41 predictions and experimental observations; see Ref. 4, p.258. However, new models, e.g. Refs. 5-6, describe observations better than K62.

Here, we show how self-similarity and anomalous scaling can coexist within the same statistics. The variables and functions we choose determine whether we observe self-similarity or only anomalous scaling. In particular, self-similarity emerges from considering the energy at scale  $\ell$ . To avoid lengthy mathematical derivations, we illustrate these ideas by an example. The example comes from a similarity theory we have developed for the inertial range.<sup>7</sup> This theory puts the inertial range pdf for Navier-Stokes turbulence within the small class of functions generated by the inverse Mellin transform of  $z^{-1} \exp(\text{sign}(\beta - 1) z^\beta)$ . One of these functions has K62 scaling exponents, namely  $\beta = 2$ . We choose this function in our example for three reasons. First, the calculations work analytically and in a closed form independent of the theory.<sup>7</sup> Second, K62 is widely known and is in reasonable agreement with observations. Third, the concepts we emphasize are shared by all functions in the class: global scaling invariance (self-similarity) emerges through the energy at scale  $\ell$  and coexists with intermittency within the same statistics.

Our example uses Mellin transforms extensively, so we review the needed properties. The Mellin transform

$$\Phi(z) = \mathfrak{M}[\phi(x); z] \equiv \int_0^\infty x^{z-1} \phi(x) dx \quad (1)$$

is useful for dealing with moments on the positive real axis. If known,  $\Phi(z)$  provides all moments including fractional orders. On the full axis, we have

$$\int_{-\infty}^\infty x^p \phi(x) dx = \mathfrak{M}[\phi(x); p+1] + (-1)^p \mathfrak{M}[\phi(-x); p+1] \quad (2)$$

However, full range moments are defined only for integer orders. Consequently, we face “Hausdorff’s moment problem,” where the integer moments do not uniquely

identify a function; see Ref. 8, p.21. For example, many functions have the same integer moments as the log-normal. In contrast, the inverse Mellin transform is unique. The Mellin transform is closely related to the Fourier transform; see Ref. 9, p.41. Each operational rule for the Fourier transform has a counterpart in the Mellin transform. We need the rule<sup>10</sup>

$$\mathfrak{M} \left[ \phi \left( (x/a)^{1/q} \right); z \right] = a^z q \Phi(qz), \quad a, q > 0. \quad (3)$$

From tables of transforms<sup>10</sup> we need the entry

$$\mathfrak{M} \left[ \frac{1}{2} \operatorname{erfc} \left( \frac{1}{2} \ln r \right); z \right] = z^{-1} e^{z^2}, \quad (4)$$

where  $\operatorname{erfc}(t) \equiv 2\pi^{-1/2} \int_t^\infty e^{-\tau^2} d\tau$  is the complementary error function.

For our example, we design a function  $F(r, \ell)$  with global scaling invariance in  $\rho = \ln r$ , but with anomalous scaling in  $r$ . The self-similarity  $F(r, \ell) = f((\rho - \mu(\ell))/\sigma(\ell))$  expresses our scaling invariance as an affine transformation on the  $\rho$ -axis. That is,  $\mu$  and  $\sigma$  reset the origin and the unit on the axis in the same way as we traditionally use mean and standard deviation. We shall call the invariance under this affine transformation ‘normal scaling’ to draw the distinction from ‘anomalous scaling.’ Anomalous scaling requires the  $p$ 'th moment of  $F(r, \ell)$  to be a power law  $C_p \ell^{\xi_p}$  where  $\xi_p$  depends nonlinearly on  $p$ . Only specific combinations of  $f(\rho)$ ,  $\mu(\ell)$ , and  $\sigma(\ell)$  permit  $F(r, \ell)$  to have anomalous scaling in  $r$ .  $f(\rho) = \frac{1}{2} \operatorname{erfc}(\frac{1}{2}\rho)$  is one such function as we shall now show. By construction, we have

$$F(r, \ell) = f \left( \frac{\ln r - \mu(\ell)}{\sigma(\ell)} \right) = f \left( \ln \left( \frac{r}{e^\mu} \right)^{1/\sigma} \right). \quad (5)$$

Using (3) we compute the moments:

$$\begin{aligned} \int_0^\infty r^p F(r, \ell) dr &= \mathfrak{M} [F(r, \ell); p+1] \\ &= \sigma e^{(p+1)\mu} \mathfrak{M} [f(\ln r); (p+1)\sigma] = \frac{e^{(p+1)\mu + (p+1)^2 \sigma^2}}{p+1}. \end{aligned} \quad (6)$$

For  $\ell \leq 1$  (small scales), we choose  $\mu(\ell) = -\alpha \ln \ell$  and  $\sigma(\ell) = \gamma \sqrt{-\ln \ell}$  so as to obtain the power laws

$$\int_0^\infty r^p F(r, \ell) dr = \frac{\ell^{-(p+1)\alpha - (p+1)^2 \gamma^2}}{p+1}. \quad (7)$$

So, the scaling in  $r$  is anomalous except when  $\gamma = 0$ .

Let us establish a connection with turbulence. Because of incompressibility, the velocity is divergence-free and consequently has only two independent components. Thus, two random variables describe isotropic turbulence at each scale. One choice is longitudinal and transverse velocity increments, i.e.,  $\delta v_{\parallel}(\ell)$  and  $\delta v_{\perp}(\ell)$ . Another is left- and right-handed velocity components obtained

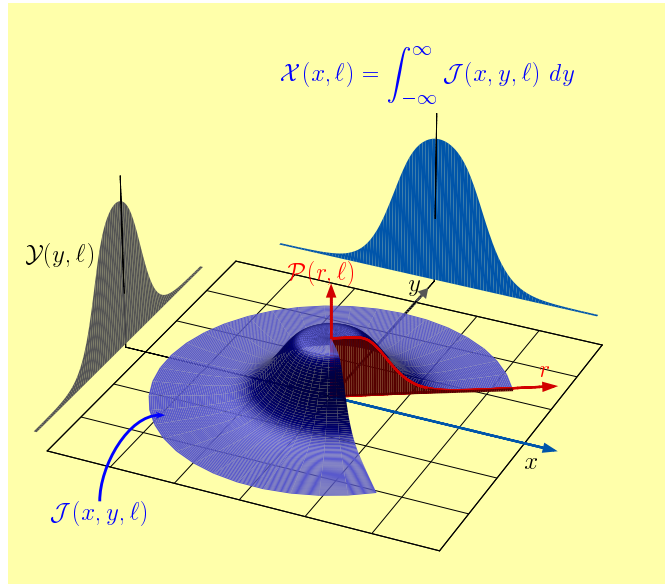


FIG. 1: (Color online) The joint pdf  $\mathcal{J}(x, y, \ell)$  is shown for  $\ell = 0.01$  together with the one dimensional pdf  $\mathcal{X}(x, \ell)$  and  $\mathcal{Y}(y, \ell)$ . The radial profile  $P(r, \ell)$  is self-similar (Fig. 2), but  $\mathcal{X}(x, \ell)$  shows anomalous scaling (Fig. 3).

via the complex helical waves decomposition.<sup>11</sup> Theoretically, we want the left-right symmetry of the Navier-Stokes equations reflected in the variables. Thus, their squares summed with equal weight should yield the energy in scale  $\ell$ . That then provides a Cartesian description. To emphasize this point, we call the two random variables  $X$  and  $Y$ . In this regard, left- and right-handed amplitudes are good variables,<sup>11</sup> but  $\delta v_{\parallel}(\ell)$  and  $\delta v_{\perp}(\ell)$  are not; see Ref. 12, p.208. Let  $\mathcal{X}(x, \ell)$  be the pdf for  $X$ , i.e.,  $\mathcal{X}(x) dx = \Pr \{x < X < x + dx\}$ . Similarly, let  $\mathcal{Y}(y, \ell)$  be the pdf for  $Y$ , and  $\mathcal{J}(x, y, \ell)$  the joint pdf for  $X$  and  $Y$ . Because  $\mathcal{J}(x, y, \ell) \rightarrow 0$  as  $x^2 + y^2 \rightarrow \infty$ , the graph of  $\mathcal{J}$  has the shape of a mountain centered near  $(0, 0)$ . Thus, we use polar coordinates  $(x, y) = r(\cos \theta, \sin \theta)$  and we obtain an azimuthal decomposition

$$\mathcal{J}(x, y) = P(r) + \cos(\theta - \theta_1)P_1(r) + \cos(2(\theta - \theta_2))P_2(r) + \dots \quad (8)$$

where  $\theta_1, \theta_2, \dots$  are phase-constants. We focus on the axisymmetric contribution to  $\mathcal{J}$ . Returning to our example, we construct  $\mathcal{J}$  from  $F(r, \ell)$ :

$$\mathcal{J}(x, y, \ell) = P(r, \ell) = C(\ell)F(r, \ell), \quad (9)$$

where the factor  $C(\ell) = 1/(2\pi \mathfrak{M}[F(r, \ell); 2]) = \pi^{-1} e^{-2\mu - 4\sigma^2}$  gives unit volume under the graph and ensures  $\mathcal{J}$  is a pdf.

With normal scaling built into  $\mathcal{J}$ , consider the situation graphically. Figure 1 shows  $\mathcal{J}(x, y, \ell)$  for  $\ell = 0.01$ . As we vary  $\ell$  the graph changes.  $\mu(\ell)$  controls the half-width-radius of the ‘‘pie,’’ while  $\sigma(\ell)$  sets the slope there.  $\mu(\ell)$  and  $\sigma(\ell)$  do not change proportionally, so statistical similarity is impossible. In the limit  $\ell \rightarrow 1^-$ , the graph looks like a disk, but as  $\ell \rightarrow 0^+$  a sharp peak develops at

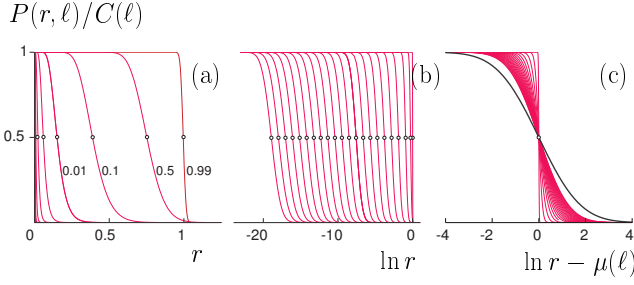


FIG. 2: (Color online) (a) The normalized radial profile  $P(r, \ell)/C(\ell) = F(r, \ell)$  for  $\ell = 0.99, 0.5, 0.1, 0.01, \dots, 10^{-20}$ ; (b) Same graphs on a logarithmic abscissa  $\rho = \ln r$ ; (c) Collapse by normal scaling  $\rho \rightarrow (\rho - \mu(\ell))/\sigma(\ell)$  to  $\frac{1}{2} \operatorname{erfc}(\frac{1}{2}\rho)$  (the heavy black graph).

$(0, 0)$ . Figure 2a shows the normalized radial profile for various  $\ell$ . For small  $\ell$ , the curves cluster near the vertical axis and are impossible to distinguish. The remedy is a logarithmic axis (Fig. 2b). On the logarithmic axis, the curves look alike so we align the midpoints (Fig. 2c). Then horizontal scaling (i.e. multiplying the abscissa by  $1/\sigma$ ) collapses all curves onto  $f(\rho) = \frac{1}{2} \operatorname{erfc}(\frac{1}{2}\rho)$ .

In contrast, the traditional analysis of the same statistics shows anomalous scaling. Two steps are involved. First, we find scaling exponents  $\zeta_p$  for the structure functions (i.e., moments) of a single random variable such as  $X$ . Second, we plot the corresponding pdf,  $\mathcal{X}(x, \ell)$ , for various  $\ell$  with the abscissa in units of  $\langle X^2 \rangle^{1/2}$  and the ordinate scaled to give unit area.

To obtain  $\zeta_p$ , we calculate the moments of  $\mathcal{X}(x, \ell)$  by integrating  $\mathcal{J}(x, y, \ell)$  over  $y$ . Using (7) and (9) we have

$$\begin{aligned} \int_0^\infty x^p \mathcal{X}(x, \ell) dx &= \int_0^\infty x^p \int_{-\infty}^\infty P(r, \ell) dy dx \\ &= \int_{-\pi/2}^{\pi/2} \int_{-\infty}^\infty (r \cos \theta)^p P(r, \ell) r dr d\theta \\ &= 2 \int_0^{\pi/2} \cos^p \theta d\theta \int_0^\infty r^{p+1} P(r, \ell) dr \\ &= K_p \mathfrak{M}[P(r, \ell); p+2] = K_p \ell^{-\alpha p - (p^2+4p)\gamma^2} \end{aligned} \quad (10)$$

where  $p > -1$  and  $K_p = \sqrt{\pi} \Gamma(\frac{p}{2} + \frac{1}{2}) / \Gamma(\frac{p}{2} + 1)$  with  $\Gamma(z)$  being the usual gamma function. (Full range moments follow from (2).) Note the  $\theta$ -integral in (10) converges only when  $p > -1$ , whereas the  $r$  integral converges for  $p > -2$ . Thus, by considering  $X$  rather than  $\sqrt{X^2 + Y^2}$  we lose all exponents in the range  $-2 < p \leq -1$ . Clearly,  $\zeta_p = -\alpha p - (p^2 + 4p)\gamma^2$ . So  $\zeta_0 = 0$  and  $\zeta_3 = -3\alpha - 21\gamma^2$ . Choosing  $\alpha = -\frac{1}{3} - 7\gamma^2$  and  $\gamma = 1/\sqrt{90}$  yields  $\zeta_3 = 1$  and  $\zeta_6 = 1.8$ . By design, our  $\zeta_p$ , shown in the inset in Fig. 3, have classical K62-values.<sup>2</sup>

Figure 3 shows the graphs of  $\mathcal{X}(x, \ell)$  for the same values of  $\ell$  as in Fig. 2. This time, the curves do not collapse to one, but exhibit the usual flaring tails associated with

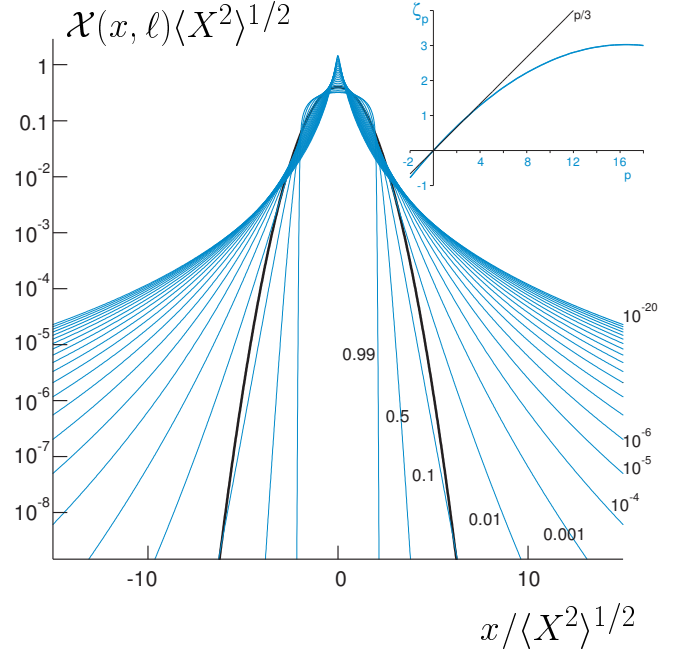


FIG. 3: (Color online) (Inset) K62 Scaling exponents; (Main figure)  $\mathcal{X}(x, \ell)$  obtained numerically from (12) for the same values of  $\ell$  as in Fig. 2.

anomalous scaling. To reveal asymptotic properties, we rewrite  $\mathcal{X}(x, \ell)$  analytically. For  $x > 0$ ,

$$\begin{aligned} \mathcal{X}(x, \ell) &= \int_{-\infty}^\infty \mathcal{J}(x, y, \ell) dy = \int_{-\infty}^\infty P(r, \ell) dy \\ &= \int_{-\pi/2}^{\pi/2} P(x \sec \theta, \ell) x \sec^2 \theta d\theta \\ &= \frac{2x}{\sqrt{\pi}} C(\ell) \int_0^{\pi/2} \int_{\frac{1}{2\sigma} \ln(e^{-\mu} x \sec \theta)}^\infty e^{-t^2} \sec^2 \theta dt d\theta \\ &= \frac{x C}{\sigma \sqrt{\pi}} \int_0^{\pi/2} \exp\left(-\frac{\ln^2(e^{-\mu} x \sec \theta)}{4\sigma^2}\right) \tan^2 \theta d\theta, \end{aligned} \quad (11)$$

where the last step requires integration by parts. Upon the substitution  $\eta = \ln \sec \theta$ , the integral becomes numerically friendly with nice asymptotic properties:

$$\mathcal{X}(x, \ell) = \frac{C e^{\mu+\sigma^2}}{\sigma \sqrt{\pi}} \int_0^\infty \sqrt{1 - e^{-2\eta}} \exp\left(-\left(\frac{\eta - \eta_c}{2\sigma}\right)^2\right) d\eta \quad (12)$$

where  $\eta_c = 2\sigma^2 - \ln x + \mu$ . For fixed  $\ell$ , we have  $\eta_c \rightarrow \infty$  as  $x \rightarrow 0^+$  and the integrand reduces to a Gaussian so that

$$\mathcal{X}(0, \ell) = \frac{C e^{\sigma^2+\mu}}{\sigma \sqrt{\pi}} \sqrt{4\pi\sigma^2} = 2\pi^{-1} e^{-3\sigma^2-\mu}. \quad (13)$$

With  $\langle X^2 \rangle^{1/2} = \frac{1}{2} e^{6\sigma^2+\mu}$ , we have  $\langle X^2 \rangle^{1/2} \mathcal{X}(0, \ell) = \pi^{-1} e^{3\sigma^2} = \pi^{-1} \ell^{-1/30} \rightarrow \infty$  as  $\ell \rightarrow 0^+$ . Thus, the peak

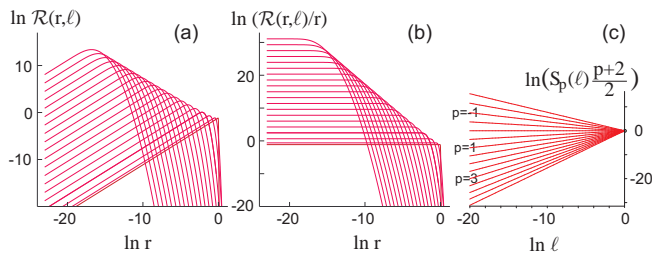


FIG. 4: (Color online) (a) The pdf for the amplitude  $\sqrt{X^2 + Y^2}$  at scale  $\ell$  with the same  $\ell$  values as in Figs. 2 and 3; (b)  $\mathcal{R}(r, \ell)/r = 2\pi P(r, \ell)$  is self-similar and collapses by normal scaling; (c) Structure functions  $S_p(\ell) = 2\ell^{\zeta_p}/(p+2)$  plotted to reveal the virtual origin for the inertial range.

in Fig. 3 rises without bound as  $\ell \rightarrow 0^+$ . Again for fixed  $\ell$ , we have  $\eta_c \rightarrow -\infty$  as  $x \rightarrow \infty$  so that the essential contribution to the integral (12) comes from a small interval to the right of  $x = 0$ . Asymptotic analysis yields:

$$\begin{aligned} \mathcal{X} &\sim \frac{2x\sigma^2}{\pi} e^{-4\sigma^2 - 2\mu} \exp\left(-\frac{\ln^2(xe^{-\mu})}{4\sigma^2}\right) \ln^{-3/2}(xe^{-\mu}) \\ &= \frac{2\gamma^2 |\ln \ell|}{\pi} \ell^{2\alpha + 4\gamma^2} x \ln^{-3/2}(x/\ell^\alpha) \exp\left(-\frac{\ln^2(x/\ell^\alpha)}{4\gamma^2 |\ln \ell|}\right) \end{aligned}$$

as  $x \rightarrow \infty$ . The decay of  $\mathcal{X}(x, \ell)$  is essentially log-normal.

We emphasize that our example is not intended as a model of intermittency, but rather as an illustration of the symmetry expressed by the global invariance of  $F(r, \ell) = P(r, \ell)/C(\ell)$  under the affine transformation  $\rho(r) = \ln r \rightarrow (\rho - \mu(\ell))/\sigma(\ell)$ . Our example is not a model because we make no modeling approximations. Rather, we suggest that equilibrium turbulence has precisely this symmetry. Considering Navier-Stokes equations with steady forcing as a dynamical system, equilibrium turbulence represents an attractor in phase space. Our suggestion is that Navier-Stokes equations restricted to the living space of the attractor obey our symmetry. Our suggestion is supported by shell model calculations<sup>7</sup> and recently by low resolution DNS in a

periodic box. Theoretically, we can show<sup>7</sup> that the symmetry exists together with anomalous scaling in  $r$  only when  $\mathfrak{M}[f(\ln r); z] = z^{-1} \exp(\text{sign}(\beta - 1)z^\beta)$ . Our preliminary DNS show  $\beta \approx 1.4$ , significantly less than two. Thus, there is no point in attempting to fix and resurrect K62.

Using our example, we illustrate how our global scaling invariance appears in analysis of data with  $J(x, y, \ell)$  statistics. With  $X^2 + Y^2$  being a random variable for the energy at scale  $\ell$ , we construct the pdf for the velocity magnitude as  $\mathcal{R}(r, \ell) dr = \Pr\{r < \sqrt{X^2 + Y^2} < r + dr\}$ . A simple and robust technique for that purpose is kernel density estimation.<sup>13</sup> Plotting the pdf on log-log scales for various  $\ell$ , we obtain Fig. 4(a). All curves have an asymptote with slope one. This is the signature of a monopole in polar coordinates, i.e.  $0 < P(0, \ell) < \infty$  implies  $\mathcal{R}(r, \ell) dr \approx 2\pi P(0, \ell) r dr$  as  $r \rightarrow 0^+$ . We make the asymptote horizontal and thus immune to abscissa scaling by considering the function  $\mathcal{R}(r, \ell)/r$ , which is  $2\pi P(r, \ell)$  so that the curves in Fig. 4b collapse to one by normal scaling. In addition, our global scaling invariance also shows up in  $S_p(\ell) \equiv \langle (\sqrt{X^2 + Y^2})^p \rangle$ . Using (5) and (9), we have  $S_p(\ell) = 2\ell^{\zeta_p}/(p+2)$ . When plotted as in Fig. 4c, all lines converge on a focal point. It is at  $(0, 0)$  because of the way we have normalized our example. The focus marks an infrared virtual origin for the inertial range. The focal abscissa is the intrinsic length scale for inertial range. The ordinate is proportional to the dissipation as in Kolmogorov's four-fifths law, but we do not yet know the proportionality constant.

Consider the juxtaposition of Figs. 2 and 3, which represent the same statistics,  $\mathcal{J}(x, y, \ell)$ . In Fig. 2 all curves collapse to one by normal scaling, while in Fig. 3 anomalous scaling prevents them from doing so. Our example is analytic and exact—no modeling or numerical issues blur the juxtaposition. Our example shows directly that intermittency is not at odds with global scaling invariance. Normal scaling on the logarithmic axis accommodates two independent parameters  $\mu(\ell)$  and  $\sigma(\ell)$ ; see Fig. 2(b)-(c). In contrast, statistical similarity allows only one and fails for that reason.

<sup>1</sup> A. N. Kolmogorov, "The local structure of turbulence in incompressible viscous fluid for very large Reynolds number," (1941), Reprinted in Proc. R. Soc. Lond. A **434**, 9 (1991).

<sup>2</sup> U. Frisch, *Turbulence*, Cambridge Univ. Press, 1995.

<sup>3</sup> A. N. Kolmogorov, "A refinement of previous hypotheses concerning the local structure of turbulence in a viscous incompressible fluid at high Reynolds number," J. Fluid Mech. **13**, 82 (1962).

<sup>4</sup> S. Pope, *Turbulent Flows*, Cambridge Univ. Press, 2000.

<sup>5</sup> Z. She and E. Leveque, "Universal scaling laws in fully developed turbulence," Phys. Rev. Lett. **72**, 336 (1994).

<sup>6</sup> T. Lundgren, "Inertial range scaling law," J. Turb. **6**, N22 (2005).

<sup>7</sup> M. Melander and B. Fabijonas, "A theory of inertial range similarity in isotropic turbulence," Technical Report 5, SMU, 2005, available at <http://arxiv.org/abs/physics/0603185>.

<sup>8</sup> T. Koerner, *Fourier Analysis*, Cambridge Univ. Press, 1988.

<sup>9</sup> I. Sneddan, *Fourier Transforms*, Dover, 1995.

<sup>10</sup> F. Oberhettinger, *Tables of Mellin Transforms*, Springer, 1974.

<sup>11</sup> M. Lesieur, *Turbulence in Fluids*, Martinus Nijhoff, 2nd edition, 1990.

<sup>12</sup> J. Hinze, *Turbulence*, McGraw-Hill, New York, 1987.

<sup>13</sup> B. Silverman, *Density Estimation*, Chapman and Hall, 1990.